# Structural Insight into Poplar Glutaredoxin C1 with a Bridging Iron−Sulfur Cluster at the Active Site[†,‡]

Yingang Feng,[§,||] Nan Zhong,[§,||] Nicolas Rouhier,[⊥] Toshiharu Hase,[#] Masami Kusunoki,[#] Jean-Pierre Jacquot,[⊥] Changwen Jin,[§,||,@] and Bin Xia*[,§,||,@]

*Beijing Nuclear Magnetic Resonance Center, Beijing 100871, People's Republic of China, College of Chemistry and Molecular Engineering, Peking University, Beijing 100871, People's Republic of China, College of Life Science, Peking University, Beijing 100871, People's Republic of China, Unité Mixte de Recherches INRA UHP 1136, Interaction Arbres Microorganismes, IFR 110 Génomique, Ecophysiologie et Ecologie Fonctionnelles, Université Henri Poincaré, BP 239, 54506 Vandoeuvre Cedex, France, and Research Center for Structural and Functional Proteomics, Institute for Protein Research, Osaka University, 3-2 Yamadaoka, Suita, Osaka 565-0871, Japan*

*Received March 6, 2006; Revised Manuscript Received April 12, 2006*

ABSTRACT: Glutaredoxins are glutathione-dependent enzymes that function to reduce disulfide bonds in vivo. Interestingly, a recent discovery indicates that some glutaredoxins can also exist in another form, an iron−sulfur protein [Lillig, C. H., et al. (2005) *Proc. Natl. Acad. Sci. U.S.A. 102*, 8168−8173]. This provides a direct connection between glutaredoxins and iron−sulfur proteins, suggesting a possible new regulatory role of iron−sulfur clusters along with the new functional switch of glutaredoxins. Biochemical studies have indicated that poplar glutaredoxin C1 (Grx-C1) is also such a biform protein. The apo form (monomer) of Grx-C1 is a regular glutaredoxin, and the holo form (dimer) is an iron−sulfur protein with a bridging [2Fe-2S] cluster. Here, we report the structural characterizations of poplar Grx-C1 in both the apo and holo forms by NMR spectroscopy. The solution structure of the reduced apo Grx-C1, which is the first plant Grx structure, shows a typical Grx fold. When poplar Grx-C1 forms a dimer with an iron−sulfur cluster, each subunit of the holo form still retains the overall fold of the apo form. The bridging iron−sulfur cluster in holo Grx-C1 is coordinated near the active site. In addition to the iron−sulfur cluster linker, helix α3 of each subunit is probably involved in the direct contact between the two subunits. Moreover, two glutathione molecules are identified in the vicinity of the iron−sulfur cluster and very likely participate in cluster coordination. Taken together, we propose that the bridging [2Fe-2S] cluster is coordinated by the first cysteine at the glutaredoxin active site from each subunit of holo Grx-C1, along with two cysteines from two glutathione molecules. Our studies reveal that holo Grx-C1 has a novel structural and iron−sulfur cluster coordination pattern for an iron−sulfur protein.

Glutaredoxins (Grxs)[1] are glutathione-dependent redox enzymes that catalyze essential biosynthetic reactions and regulate many biological processes (*1*). Grxs can reduce protein disulfide bonds or protein−glutathione mixed disulfide bonds. To date, the biochemical and structural studies of Grxs have been mainly focused on *Escherichia coli*, yeast, and mammalian Grxs, and a number of structures of Grxs from these species have been resolved (*2*−*9*). Like thioredoxins, various isoforms of Grxs are present in most living organisms (*10*). The number of Grx isoforms in plants is much larger than the number in other organisms, and this probably indicates important roles for glutaredoxins in plants (*11, 12*). However, the research on plant Grxs is still very limited, and there is no plant Grx structure available to date.

According to the active site sequences, plant Grxs have been classified into three major types: the CPYC type, the CGFS type, and the CC type (*11*). The CPYC type and CGFS type Grxs also exist in other organisms, while the CC-type Grxs appear to be specific to higher plants. There are also some Grxs with atypical active site sequences, such as CSYS, CGYC, CSYC, etc.

Recently, it was reported that human Grx2 (with a CSYC active site) exists in two different forms. It is a regular glutaredoxin in the monomeric form, and it is also present as an iron−sulfur protein with a bridging [2Fe-2S] cluster

[†] This research was supported by Grants 30125009 and 30570353 to B.X. and Grant 30325010 to C.J. from the National Science Foundation of China and a research grant from the China Postdoctoral Science Foundation to Y.F. A BQR Region grant to N.R. from University Henri Poincare is acknowledged. J.-P.J. and B.X. also acknowledge the funding from the Programme de Recherches Avancées (PRA) Franco-Chinois (BT-05 03).

[‡] The structural coordinates and all restraints for apo Grx-C1 have been deposited in the RCSB Protein Data Bank as entries 1Z7P (ensemble of 20 structures) and 1Z7R (mean structure).

* To whom correspondence should be addressed: Beijing Nuclear Magnetic Resonance Center, Peking University, Beijing 100871, China. Telephone: +86-10-62758127. Fax: +86-10-62753790. E-mail: binxia@pku.edu.cn.

[§] Beijing Nuclear Magnetic Resonance Center.

[||] College of Chemistry and Molecular Engineering, Peking University.

[⊥] Université Henri Poincaré.

[#] Osaka University.

[@] College of Life Science, Peking University.

[1] Abbreviations: Grx, glutaredoxin; GSH, glutathione; ISC, iron−sulfur cluster; Trx, thioredoxin; DTT, dithiothreitol; DSS, 2,2-dimethylsilapentane-5-sulfonic acid; NOE, nuclear Overhauser effect; HSQC, heteronuclear single-quantum coherence.

10.1021/bi060444t CCC: $33.50 
Published on Web 06/07/2006

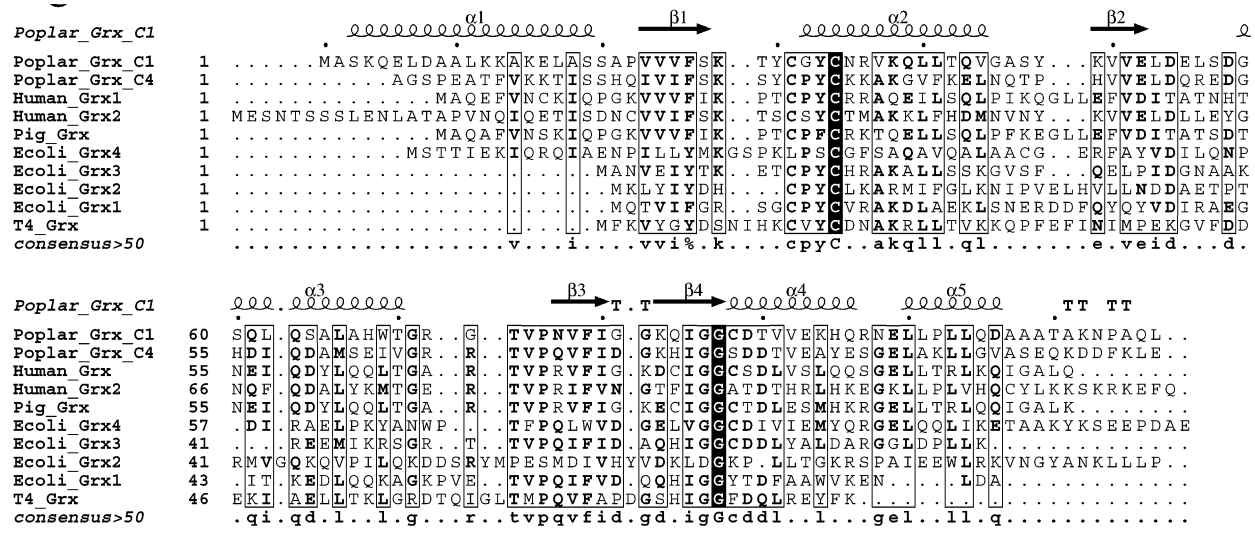


FIGURE 1: Amino acid sequence alignment of Grxs. Sequences were aligned using ClustalW (*40*) and represented using ESPript (*41*). Only the N-terminal sequence of *E. coli* Grx2 is shown for comparison. Secondary structure elements of poplar Grx-C1 are indicated at the top.

in a dimeric form. The iron−sulfur cluster (ISC) was proposed to serve as a redox sensor for the activation of this Grx (*13*). Iron−sulfur proteins are found in all life forms; most of them act as electron carriers, while some of the iron−sulfur clusters serve as catalytic centers, regulators, and sensors (*14*−*17*). Although it has been reported that glutaredoxins are involved in the ISC assembly of iron−sulfur proteins (*18*, *19*), human Grx2 is the first protein reported to be both a glutaredoxin and an iron−sulfur protein. This finding strongly suggests a more direct connection between glutaredoxins and iron−sulfur protein families.

Poplar Grx-C1 from *Populus tremula* × *tremuloides* contains 117 amino acid residues and has a CGYC active site (Figure 1). Like human Grx2, poplar Grx-C1 has been found to exist not only as a monomer (apo form) with glutaredoxin activities but also as a dimer (holo form) with a bridging [2Fe-2S] iron−sulfur cluster, which was confirmed by extended X-ray absorption fine structure (EXAFS) spectroscopy and other spectroscopic studies (N. Rouhier et al., manuscript to be submitted for publication). However, the cysteines proposed to coordinate the ISC in human Grx2 are not conserved, and they are not present in poplar Grx-C1 (*13*). Therefore, the ISC coordination pattern in poplar Grx-C1 should be different from that of human Grx2. Human Grx2 and poplar Grx-C1 are the only two proteins known to be both glutaredoxin and iron−sulfur protein. It is still not clear why these two Grxs can dimerize and become iron−sulfur proteins while others cannot. Here, we report the solution structure of the reduced apo poplar Grx-C1, the first plant Grx structure, along with the structural characterization of the iron−sulfur protein form of poplar Grx-C1 by NMR spectroscopy.

## EXPERIMENTAL PROCEDURES

*Sample Preparation.* The apo form of poplar Grx-C1 was expressed and purified according to the procedure described previously (*20*). The NMR sample contained ∼1 mM uniformly $^{13}C$- and $^{15}N$-labeled protein in 40 mM potassium phosphate buffer with 90% $H_2O$/10% $D_2O$ at pH 6.4, along with 40 mM DTT, 0.01% $NaN_3$, and 0.01% DSS, with Complete, an EDTA-free protease inhibitor cocktail (Roche). Oxygen was removed from the sample buffer by repeated vacuuming and argon gas purging to stabilize the sample.

To express poplar holo Grx-C1, the bacteria were cultured in 2 L of LB medium at 37 °C. When the $OD_{600}$ of the culture reached 0.6, the cells were collected by centrifugation and resuspended in 500 mL of M9 medium with additional 20 $\mu$M $FeCl_3$. After incubation for 30 min at 37 °C, protein expression was induced by addition of 100 $\mu$M IPTG. The bacteria were harvested 4 h later and resuspended in 25 mL of 50 mM Tris-HCl buffer (pH 7.0). The cells were first lysed by freezing and thawing, followed by sonication. The supernatant of cell lysate was applied onto a Q-Sepharose Fast Flow anion exchange column (Amersham, Uppsala, Sweden) at pH 7.0. The flow-through fraction was collected, and the pH was adjusted to 5.0 before the sample was loaded onto an SP-Sepharose Fast Flow cation exchange column. The protein was eluted using a linear pH gradient from 5.0 to 6.4 and was further purified by gel filtration with a Superdex 75 column (Amersham). The brown fraction was the holo protein. The yield of the holo protein was ∼50 mg/L of culture. The protein sample with an $A_{430}/A_{280}$ ratio of >0.38 was considered to be more than 95% pure.

*NMR Spectroscopy.* All NMR experiment data were collected at 293 K on a Bruker Avance 500 MHz spectrometer with a triple-resonance cryoprobe or a Bruker Avance 600 MHz spectrometer with a triple-resonance probe. Proton chemical shifts were referenced to internal DSS. $^{15}N$ and $^{13}C$ chemical shifts were referenced indirectly to DSS (*21*). $^{1}H$, $^{15}N$, and $^{13}C$ resonance assignments of apo Grx-C1 have been reported (*20*). Three-dimensional (3D) $^{15}N$-edited NOESY-HSQC and 3D $^{13}C$-edited NOESY-HSQC spectra were collected with mixing times of both 120 and 60 ms. A 3D $^{13}C$-edited NOESY-HSQC spectrum for the aromatic carbons was also recorded.

The backbone assignments of holo Grx-C1 were obtained on the basis of two-dimensional (2D) $^{1}H-^{15}N$ HSQC, 3D HNCA, CBCA(CO)NH, HNCO, and HN(CA)CO spectra. 2D $^{1}H-^{15}N$ HSQC, $^{1}H-^{15}N$ TOCSY-HSQC, $^{1}H-^{1}H$ TOCSY, and $^{1}H-^{1}H$ DQF-COSY spectra were used in identifying

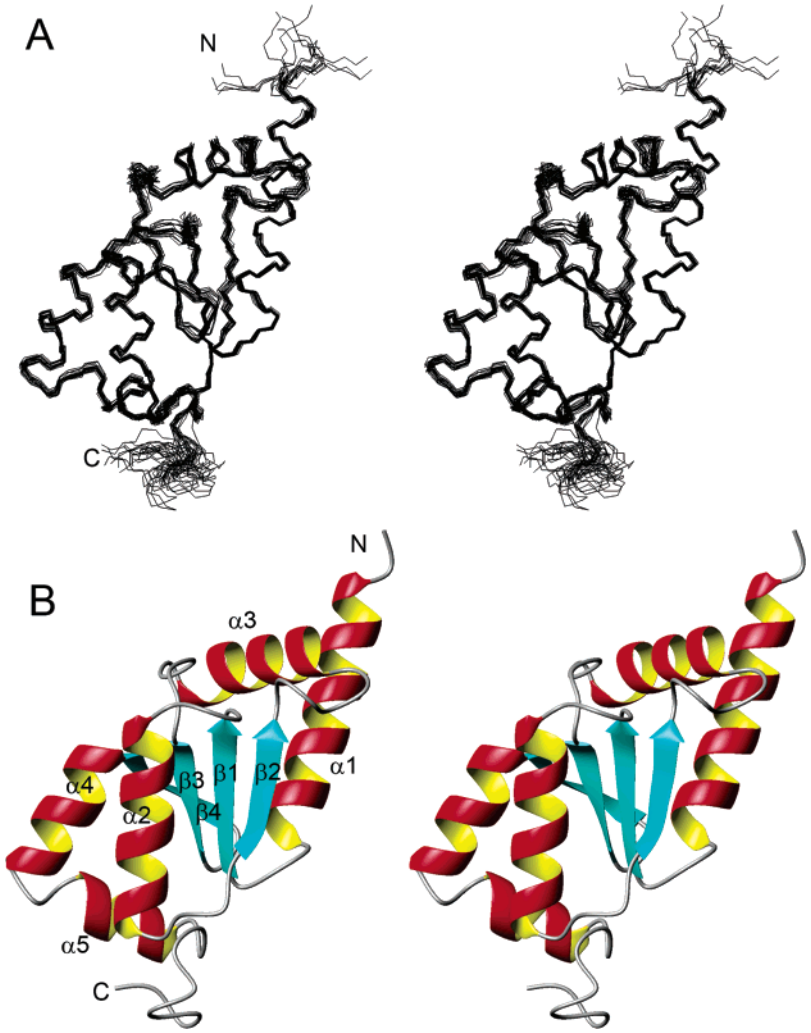


FIGURE 2: Solution structure of reduced poplar apo Grx-C1. (A) Stereoview of the backbone superimposition of 20 structures. (B) Stereoview of the ribbon representation of the mean structure.

glutathione. All NMR spectra were processed using NMRPipe (*22*) and analyzed using NMRView (*23*).

A simple delay−90°−acquisition pulse sequence was employed in collecting the one-dimensional (1D) $^1$H NMR spectra of the hyperfine-shifted signals for the holo protein; 2048 data points were digitized (500 ppm spectral width) with a cycling time of 13 ms. All 1D hyperfine NMR spectra were processed and analyzed using XWINNMR version 3.5 (Bruker).

*Structure Calculations*. Initial structures were generated using CYANA with restraints from the CANDID module (*24*). Distance restraints were derived from NOESY spectra with a mixing time of 120 ms. These initial structures were then used as filter models for SANE (*25*) to obtain further NOE assignments, and the new distance restraints were then used for another round of CYANA calculation. Dihedral angle restraints ($\phi$ and $\psi$) and hydrogen bond restraints were also used for the structure calculation. Dihedral angle restraints were obtained using TALOS (*26*). Hydrogen bond restraints were added according to the secondary structures predicted on the basis of chemical shifts and NOEs.

When the lowest CYANA target function value was smaller than 0.5 Å$^2$ and the number of NOE violations was less than five, a total of 200 structures were calculated using CYANA and the 100 structures with the lowest target function values were selected for refinement with AMBER 7 (*27*). Again, SANE was used to assist in NOE assignment. The top 20 structures with the lowest AMBER energy were selected for final analysis. The mean structure was generated using MOLMOL (*28*) and was energy minimized with AMBER.

*Structure Analysis and Homologous Modeling*. The quality of structures was analyzed using MOLMOL and PROCHECK-NMR (*29*). The figures of structures and electrostatic surfaces were prepared using MOLMOL. Homologous modeling of human Grx2 was performed using the SWISS-MODEL server (*30*).

*pH Titration and p$K_a$ Estimation*. The NMR sample for pH titration contained ~0.3 mM uniformly $^{15}$N-labeled apo protein. The pH of the sample was adjusted using HCl.

Overall, 10 2D $^1$H−$^{15}$N HSQC spectra were recorded at different pH values. The p$K_a$ values were estimated by fitting the chemical shift data to the Henderson−Hasselbach equation

$$\delta = \delta_{HA} - (\delta_{HA} - \delta_A)/(1 + 10^{pK_a - pH})$$

where $\delta$ is the measured $^1H^N$ or $^{15}N^H$ chemical shift and $\delta_{HA}$ and $\delta_A$ are the corresponding $^1H^N$ or $^{15}N^H$ chemical shifts of the protonated and deprotonated side chains, respectively.

Table 1: Restraints and Structure Statistics

| | |
|---|---|
| conformational restraints (no.) | |
| NOE restraints | 4845 |
| intraresidue | 1257 |
| sequential | 791 |
| medium-range | 617 |
| long-range | 800 |
| ambiguous | 1380 |
| dihedral angle restraints | 160 |
| $\phi$ | 79 |
| $\psi$ | 81 |
| hydrogen bond restraints | 47 |
| chirality restraints | 403 |
| $\omega$ angle | 116 |
| side chain | 287 |
| structure statistics of final 20 conformers | |
| violations [no. (maximum violation)] | |
| distance restraints | 5 (0.198 Å) |
| dihedral angle restraints | 0 |
| rmsd | |
| backbone heavy atoms | 0.88,[a] 0.32[b] |
| all heavy atoms | 1.13,[a] 0.68[b] |
| PROCHECK | |
| most favored regions (%) | 88.8 |
| additionally allowed regions (%) | 10.7 |
| generously allowed regions (%) | 0.5 |
| disallowed regions (%) | 0.0 |

[a] All residues. [b] Regular secondary structure.

## RESULTS

*Solution Structure of Apo Grx-C1*. High-quality structures were obtained for the reduced apo poplar Grx-C1. A superimposition of the final 20 conformers with the lowest AMBER energies, together with the ribbon representation of the mean structure showing the secondary structure elements, is shown in Figure 2. A summary of restraints used in structure calculations and statistics for the structure ensemble is listed in Table 1. Both trans and cis conformations were observed for the N113−P114 peptide bond, and the trans conformation is the major form. Therefore, only the trans conformation restraints were used in the structure calculations. It has been shown that the N-terminal cysteine of the Grx active site is a thiolate anion at physiological pH (*9*, *31*−*33*). Hence, thiolate C31 is used during the structure determinations.

Residues 4−110 of the apo poplar Grx-C1 fold into a compact structure, whereas the first three residues and the last seven residues are unstructured. The first two residues were invisible for NMR, while the peaks of C-terminal residues are strong and sharp with only intraresidue or sequential NOEs. The reduced poplar apo Grx-C1 exhibits a typical thioredoxin/glutaredoxin fold, and the structure comprises five α-helices (α1, residues 4−19; α2, residues 32−44; α3, residues 59−70; α4, residues 88−96; and α5, residues 100−106) and four $\beta$-strands ($\beta$1, residues 23−27; $\beta$2, residues 49−52; $\beta$3, residues 77−80; and $\beta$4, residues 83−87) with an α1−$\beta$1−α2−$\beta$2−α3−$\beta$3−$\beta$4−α4−α5 sequential connectivity (Figure 2B). The four $\beta$-strands form a mixed $\beta$-sheet. Strands $\beta$1 and $\beta$2 are parallel; strand $\beta$3 is antiparallel with $\beta$1 and $\beta$4. Helices α1 and α3 pack on one side of the $\beta$-sheet, while α2, α4, and α5 are on the other side. The packing of the sandwichlike fold is mainly contributed by the hydrophobic interactions between the sheet and helices.

*$pK_a$ of the First Active Site Cysteine.* For glutaredoxins, it is reported that the first cysteine thiolate at the Grx active site has a p$K_a$ value significantly lower than that of a free cysteine, and the p$K_a$ is a key determinant of the reactivity of the thiol (*31*, *32*). We measured the p$K_a$ value by monitoring the NH peak chemical shift changes in the 2D $^1$H−$^{15}$N HSQC spectra. Since the protein precipitated below pH 4.8, the approximate p$K_a$ value is estimated from the data obtained between pH 4.83 and 7.03. Apparently, the pH-dependent chemical shift changes of residues 31−34 are significantly larger than those of other residues (Figure 3). In addition, unlike other residues, the chemical shift changes of residues 31−34 are nonlinear in this pH range. It is assumed that the $^1H^N$ and $^{15}N^H$ chemical shift changes of residues 31−34 are mainly caused by the protonation of the C31 thiolate nearby. The estimated p$K_a$ values of C31 thiolate are listed in Table 2, ranging from 4.4 to 4.9, which are significantly larger than those of human Grx1 (∼3.5) (*32*) and pig Grx (∼3.8) (*34*).

*Characterization of Holo Grx-C1*. The backbone chemical shift assignments were determined for holo Grx-C1. Almost all the backbone amide signals in the 2D $^1$H−$^{15}$N HSQC spectrum were assigned for the holo protein (Figure 4). In the HSQC spectrum, only one set of peaks was observed, except that the C-terminal residues have small satellite peaks due to the isomerization of the N113−P114 peptide bond, the same as that of apo Grx-C1. This indicates that the two subunits are symmetric in the holo protein.

The paramagnetic effect of the [2Fe-2S] cluster would cause signals broadened and shifted for residues close to the cluster and thus would result in these signals being undetectable in normal NMR experiments. For holo Grx-C1, we were able to assign the backbone NH resonances from 100 of 113 non-proline residues. Besides the three N-terminal residues that were also not observed in the 2D $^1$H−$^{15}$N HSQC spectrum of apo Grx-C1, residues K28, Y30, C31, G32, Y33, C34, N35, R36, S57, and V75 are completely missing in the 2D $^1$H−$^{15}$N HSQC spectrum of holo Grx-C1 (Figure 5). Similarly, the $C^\alpha$ chemical shifts of most residues were obtained for holo Grx-C1 except residues Y30, C31, G32, Y33, C34, N35, and V75. Most of these residues with missing signals are located at or near the Grx active site in the apo Grx-C1 structure, except S57.

A comparison of the 2D $^1$H−$^{15}$N HSQC spectra of apo and holo Grx-C1 is shown in Figure 4. Most of the peaks from holo Grx-C1 can overlap with those from apo Grx-C1. The $^1$H and $^{15}$N combined chemical shift differences ($\delta$) between the apo and holo forms are plotted in Figure 5A. Among the 100 residues that have been assigned, $\delta$ values of 77 residues are less than 0.1 ppm (<0.05 ppm for 48 residues) which means no significant chemical shift deviation. There are only 12 residues with large chemical shift changes (>0.15 ppm): F26, T29, K38, Q61, S64, R72, N77, G87, C88, D89, T90, and V92. Also, the $C^\alpha$ chemical shift differences between the holo and apo forms are quite small for most residues (<0.2 ppm for 95 residues) (Figure 5B). We also compared the ratios of normalized peak intensities between apo and holo Grx-C1, and residues K4, K12, V25, V37, K38, L53, T74, C88, D89, and T90 exhibit significant intensity changes (Figure 5C).

*Reduction and Disassembly of the ISC with Dithionite*. Hyperfine-shifted $^1$H signals were observed in the 1D $^1$H

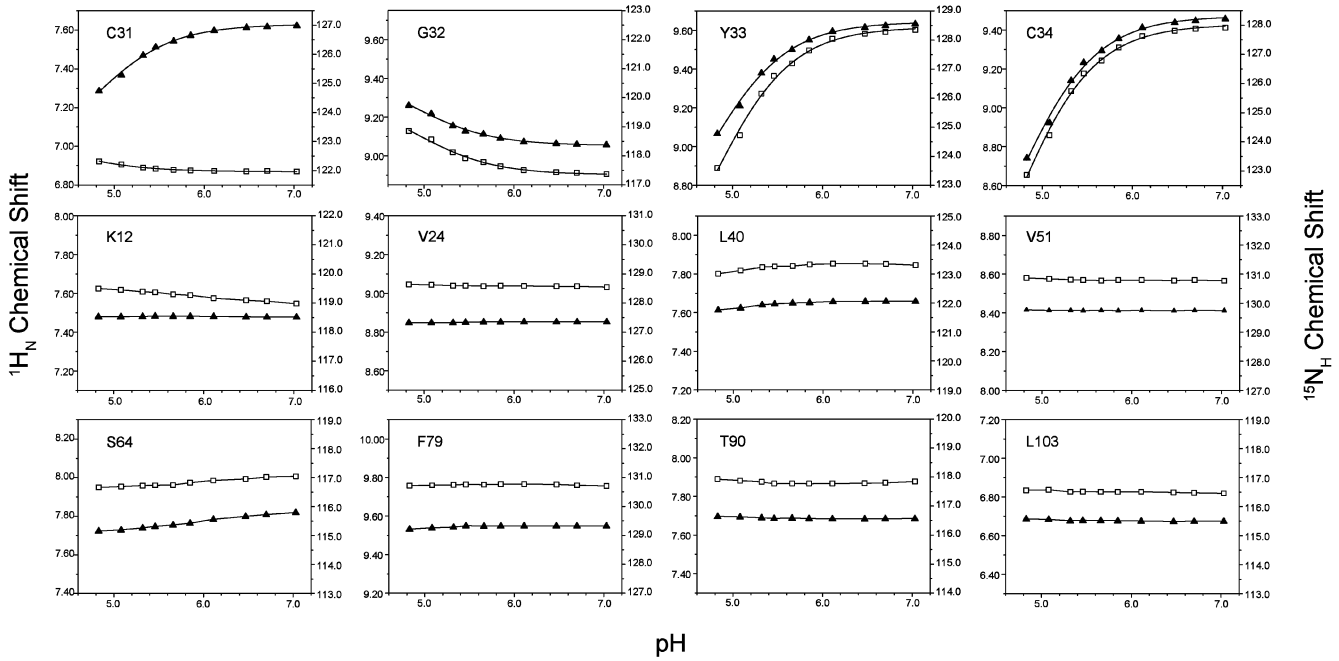


FIGURE 3: pH titration of poplar Grx-C1. White squares are for $^1H^N$ chemical shifts, and black triangles are for $^{15}N^H$ chemical shifts. For residues 31−34, the lines are the fitting curves and the correlation coefficients for all fittings are greater than 0.99. For the other residues, the lines are a simple connection of the data points.

Table 2: Estimated C31 Thiolate p$K_a$ Values from $H^N$ and $N^H$ Atoms of Residues 31−34

| | from $H^N$ | from $N^H$ | | from $H^N$ | from $N^H$ |
|---|---|---|---|---|---|
| C31 | 4.42 ± 0.17 | 4.76 ± 0.07 | Y33 | 4.78 ± 0.07 | 4.73 ± 0.07 |
| G32 | 4.91 ± 0.07 | 4.87 ± 0.07 | C34 | 4.69 ± 0.07 | 4.72 ± 0.08 |

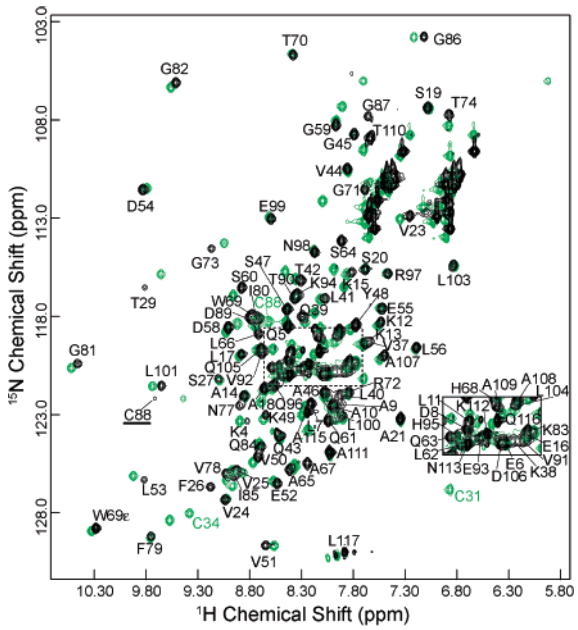


FIGURE 4: Overlay of 2D $^1H-^{15}N$ HSQC spectra of holo (black) and apo (green) poplar Grx-C1. The assignments of the holo form are labeled in black. The assignments for the three cysteines of the apo form are colored green. The weak peak of C88 observed in the HSQC spectrum of the holo form is denoted with an underlined label.

NMR spectrum of holo Grx-C1 (Figure 6). Three broad hyperfine-shifted $^1H$ peaks appeared in the 15−50 ppm region. Attempts to reduce the [2Fe-2S] cluster by introducing 2 mg of solid sodium dithionite into the NMR sample under anaerobic conditions resulted in no change in the 1D $^1H$ NMR spectrum (data not shown). The 2D $^1H-^{15}N$ HSQC spectra of holo Grx-C1 were also identical before and after addition of dithionite (data not shown). Thus, unlike most other [2Fe-2S] proteins such as ferredoxins, the ISC of holo Grx-C1 cannot be reduced by dithionite. One possible reason for this is that the redox potential for the ISC of holo Grx-C1 is unusual and the cluster is beyond reduction by dithionite. The dithionite-treated sample was stable under argon for at least 1 week.

Surprisingly, if oxygen was not pre-removed from the sample buffer, adding dithionite to the holo Grx-C1 sample resulted in the loss of the brown color in a few minutes, and white precipitate formed in the sample. Therefore, the [2Fe-2S] cluster was lost due to dithionite under this condition. After the precipitate had been removed, the NMR spectra of the remaining sample solution exhibited signals mainly from a small molecule, while most of the protein signals were missing. This indicates that the precipitate is mainly the protein. In the 2D $^1H-^{15}N$ HSQC spectrum, only two sharp peaks were observed, suggesting that this small molecule is labeled with $^{15}N$ and should be copurified with holo Grx-C1 (Figure 7A).

To identify the small molecule, the 2D $^1H-^{15}N$ TOCSY-HSQC spectrum (Figure 7B) for a $^{15}N$-labeled sample and 2D $^1H$ TOCSY (Figure 7C) and DQF-COSY spectra for an unlabeled sample were recorded. Analysis of these NMR spectra revealed that the small molecule is reduced glutathione (GSH). The assigned $^1H$ chemical shifts agreed with the published chemical shift values of GSH (*35*). However, no signal from GSH was observed in the 2D $^1H-^{15}N$ HSQC spectrum of holo Grx-C1 before the cluster fell off. Furthermore, adding DTT to holo Grx-C1 caused no difference in the 2D $^1H-^{15}N$ HSQC spectrum (data not shown), indicating that the GSH does not form a disulfide bond with cysteine residues of the protein.

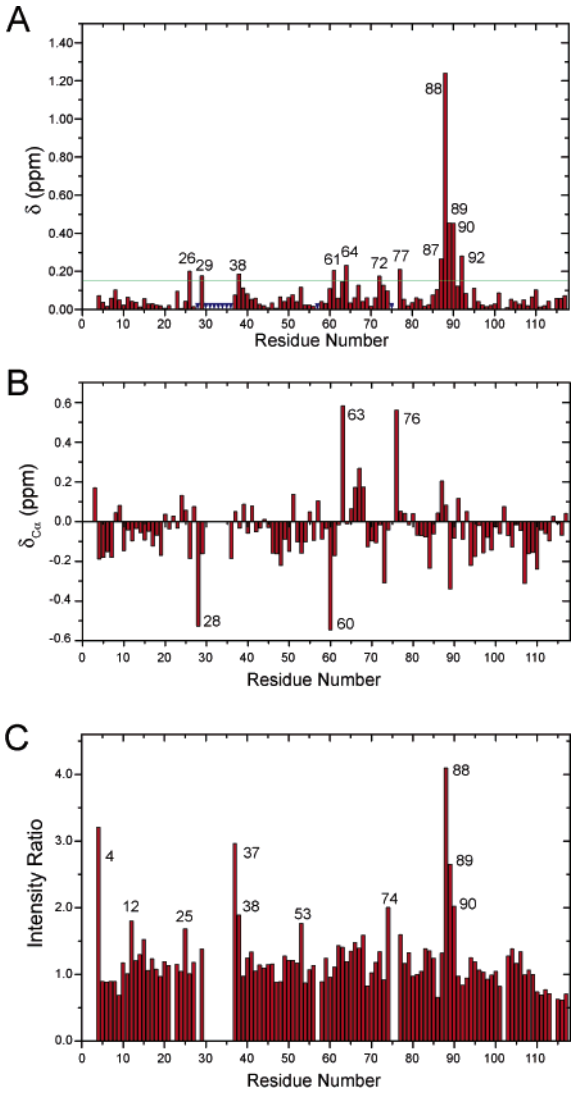


FIGURE 5: (A) $^1$H and $^{15}$N combined chemical shift differences, $\delta$, vs residue number. $\delta = [\delta_{HN}^2 + (\delta_N/6.5)^2]^{1/2}$ (*42*), in which $\delta_{HN}$ and $\delta_N$ are the chemical shift differences between the apo and holo forms for amide proton and nitrogen, respectively. Blue triangles denote the residues not observed in the HSQC spectra of the holo form. (B) $C_\alpha$ chemical shift differences ($\delta_{C_\alpha}$) between holo and apo Grx-C1 vs residue number. (C) Ratios of normalized intensities of 2D $^1$H−$^{15}$N HSQC peaks between apo and holo Grx-C1 vs residue number. Residues with large chemical shift changes or large intensity changes are indicated by their residue numbers.

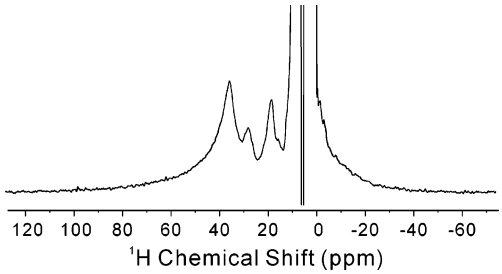


FIGURE 6: Hyperfine-shifted 1D $^1$H NMR spectrum of holo Grx-C1.

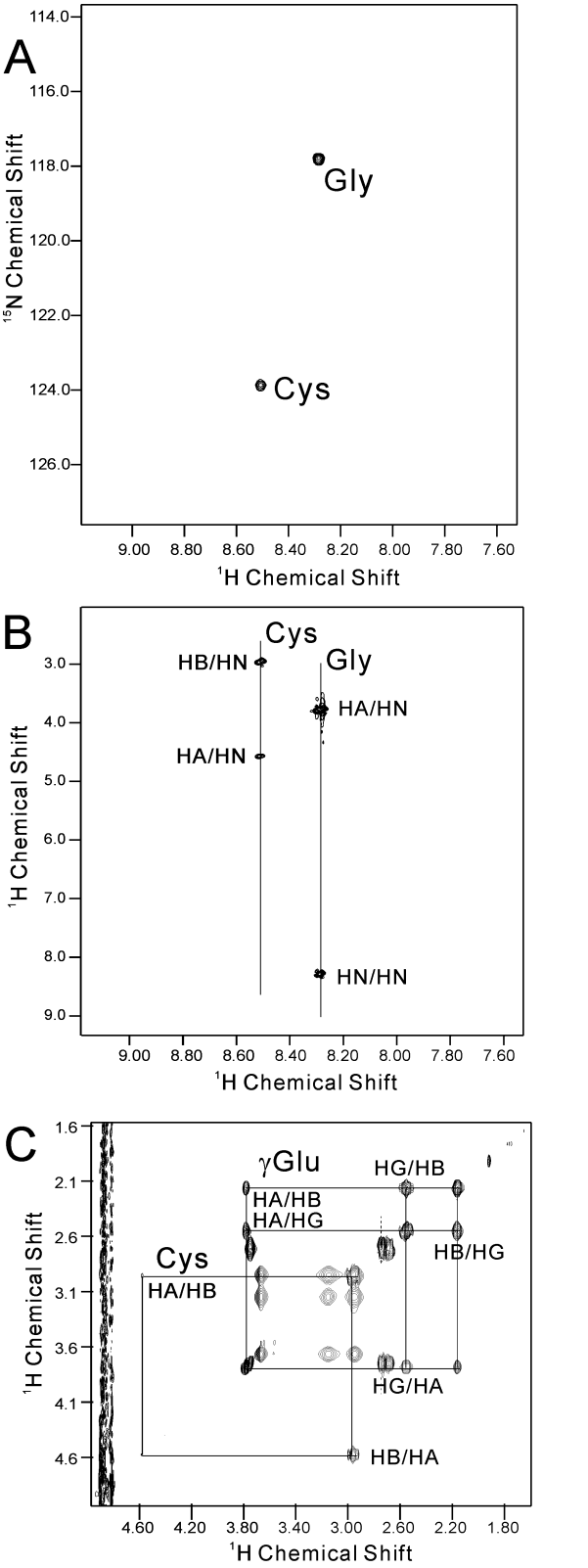


FIGURE 7: 2D $^1$H−$^{15}$N HSQC (A), 2D $^1$H−$^{15}$N TOCSY-HSQC (B), and 2D $^1$H−$^1$H TOCSY (C) spectra of GSH which falls off from holo Grx-C1. Peaks from one spin system are connected by lines.

The number of GSH molecules per holo Grx-C1 molecule was estimated using 1D $^1$H NMR spectroscopy. The holo protein concentration of the sample is ∼0.72 mM, as determined by $A_{280}$ according to the predicted extinction coefficient. The concentration of GSH was 1.65 mM, as determined by comparing the integral of the peak from $^1H^\beta$ of the glutamate residue of GSH and that of methyl protons of sodium acetate (1 mM) added to the sample. Therefore, the ratio of GSH to holo protein is ∼2.3 (1.65/0.72), which indicates that there should be two GSH molecules in one

holo Grx-C1 molecule when the experimental uncertainties are considered.

## DISCUSSION

*Structural Comparison with Other Grxs*. The solution structure of the reduced apo poplar Grx-C1 is the first plant Grx structure. Although all Grxs with known structures adopt a typical Trx fold, the structure of poplar Grx-C1 is more similar to that of the mammalian Grxs than the others. The backbone heavy atom rmsd between poplar Grx-C1 and human Grx1 is ~1.4 Å. The only one significant difference is that the N-terminal helix of poplar Grx-C1 is much longer than those of mammalian Grxs (Figure 8A). Most *E. coli* and phage T4 Grxs lack the corresponding N-terminal and/or C-terminal helices. However, all plant Grxs may have the same core structure of five α-helices and four β-strands as poplar Grx-C1 according to the sequence alignment of plant Grx isoforms (data not shown).

The active site conformation of poplar Grx-C1 is also quite similar to that of human Grx1 (Figure 8B). The major difference between them is the side chain of the first active site cysteine. Among the 20 conformers, the $\chi_1$ angles of the first active site cysteine in human Grx1 mainly show a trans conformation, while those of poplar Grx-C1 mostly adopt a g+ conformation. Comparison of the surface electrostatic distributions between poplar Grx-C1 and human Grx1 shows that the active site regions for both proteins are similarly positively charged (Figure 8C). However, it is less positively charged around the first active site cysteine thiolate in poplar Grx-C1 than in human Grx1. For human Grx1, this thiolate is surrounded by four positively charged residues (K20, R28, R68, and R72), whereas for poplar Grx-C1, three positively charged residues (K28, R36, and R72) are located on one side of C31 thiolate and two negatively charge residues (D54 and D55) are on the other side, away from the active site (Figure 8C). The difference in charge distributions could well explain why the p$K_a$ value of N-terminal active site cysteine of poplar Grx-C1 is higher than that of human Grx1, since the thiolate p$K_a$ values of Grxs have been attributed to the peripheral charges (*9*, *36*).

*Structural Insight of Holo Grx-C1*. Since most peaks in the 2D $^1H-^{15}N$ HSQC spectrum of the holo Grx-C1 can be superimposed on those of apo Grx-C1 (Figure 4), the structure of each subunit of holo Grx-C1 should be very similar to that of the apo form. This can be demonstrated more clearly by mapping the residues without significant chemical shift deviations ($\delta$ < 0.1 ppm) on the apo Grx-C1 structure (Figure 9A). Apparently, the residues without significant chemical shift changes are distributed in all secondary structure elements. Thus, when two apo Grx-C1 molecules are linked by a [2Fe-2S] cluster and become an iron−sulfur protein, no significant structural change occurs and each subunit of holo Grx-C1 retains the overall fold of apo Grx-C1. Therefore, the structure of apo Grx-C1 can be used to obtain further structural information about the holo protein.

The paramagnetic effect of the iron−sulfur cluster will cause NMR signals to be broadened and/or hyperfine-shifted for residues close to the cluster. For rubredoxin, which has a single iron cluster, backbone NH signals from residues within 8 Å of the iron are severely broadened and are beyond detection for regular NMR experiments (*37*). The backbone NH group located between 8.5 and 11 Å from the iron would also experience NMR signal broadening, but some of them can still be detected in the 2D $^1H-^{15}N$ HSQC experiment. However, their peaks have much weaker intensities and sometimes are also shifted. Therefore, the information about missing signals and weakened signals can be used to locate the position of the [2Fe-2S] cluster in holo Grx-C1. In the 2D $^1H-^{15}N$ HSQC spectrum of holo Grx-C1, the backbone NH signals from 10 residues are missing. When these missing residues are mapped on the structure, it is found that most of them are located at or near the Grx active site, except S57 (Figure 9B, red spheres). Since the NH peak of S57 is also very weak in apo Grx-C1, the loss of this peak in the holo protein is probably caused by dynamics. On the other hand, the other missing residues are clustered together, and the loss of their NH signals should be due to the paramagnetic effect of the [2Fe-2S] cluster. These residues should be located in the vicinity of the ISC. In another sense, the [2Fe-2S] cluster must be coordinated near the glutaredoxin active site.

Besides the missing residues, there are also some residues that exhibit large chemical shift and/or peak intensity changes in the HSQC spectrum of holo Grx-C1. These changes could be mainly attributed to two reasons. One is the paramagnetic effect of the ISC, and the other is the direct contact between two subunits. Signals affected by the paramagnetic effect would have chemical shift changes and weaker peak intensities, while the direct contact between two subunits will mainly cause the chemical shift changes. When the residues with large chemical shift changes and/or peak intensity changes are mapped on the apo Grx-C1 structure, we found that most of these residues are around the active site as expected, except residues K4, K12, S60, Q61, Q63, and S64 (Figure 9B). Since residues K4 and K12 are scattered in the mapping and distant from the Grx active site, their intensity changes are probably not due to the paramagnetic effect. Residues S60, Q61, Q63, and S64 are on one region of helix α3 which is a bit far from the active site. They have large chemical shift changes but no significant intensity changes. Therefore, helix α3 may be involved in direct contact between two subunits.

*Coordination of the ISC*. Normally, a [2Fe-2S] cluster is coordinated by four sulfur atoms from cysteines. Because of the paramagnetic effect of the ISC, the residues involved in the cluster coordination will not be observable in the HSQC spectrum. In one holo Grx-C1 molecule, there are eight cysteines: three from each subunit (C31, C34, and C88) and two from the two GSH molecules. Among these cysteines, C88 can be excluded as the ligands of ISC since its peak can be observed in the HSQC spectrum of holo Grx-C1 (Figure 4). The GSHs cannot be observed in the HSQC spectrum of holo Grx-C1. This suggests that the GSHs in holo Grx-C1 are close to the ISC. In addition, the GSHs cannot be released from holo Grx-C1 by DTT treatment, and they were freed after the ISC fell off. These indicate that the GSHs are not covalently attached to the protein, and their cysteines do not form disulfide bonds with the protein subunits. Therefore, the most reasonable explanation for the involvement of GSHs in holo Grx-C1 is that the two GSH molecules participate in the ISC coordination. Since two GSHs only provide two cysteines, the other two coordination

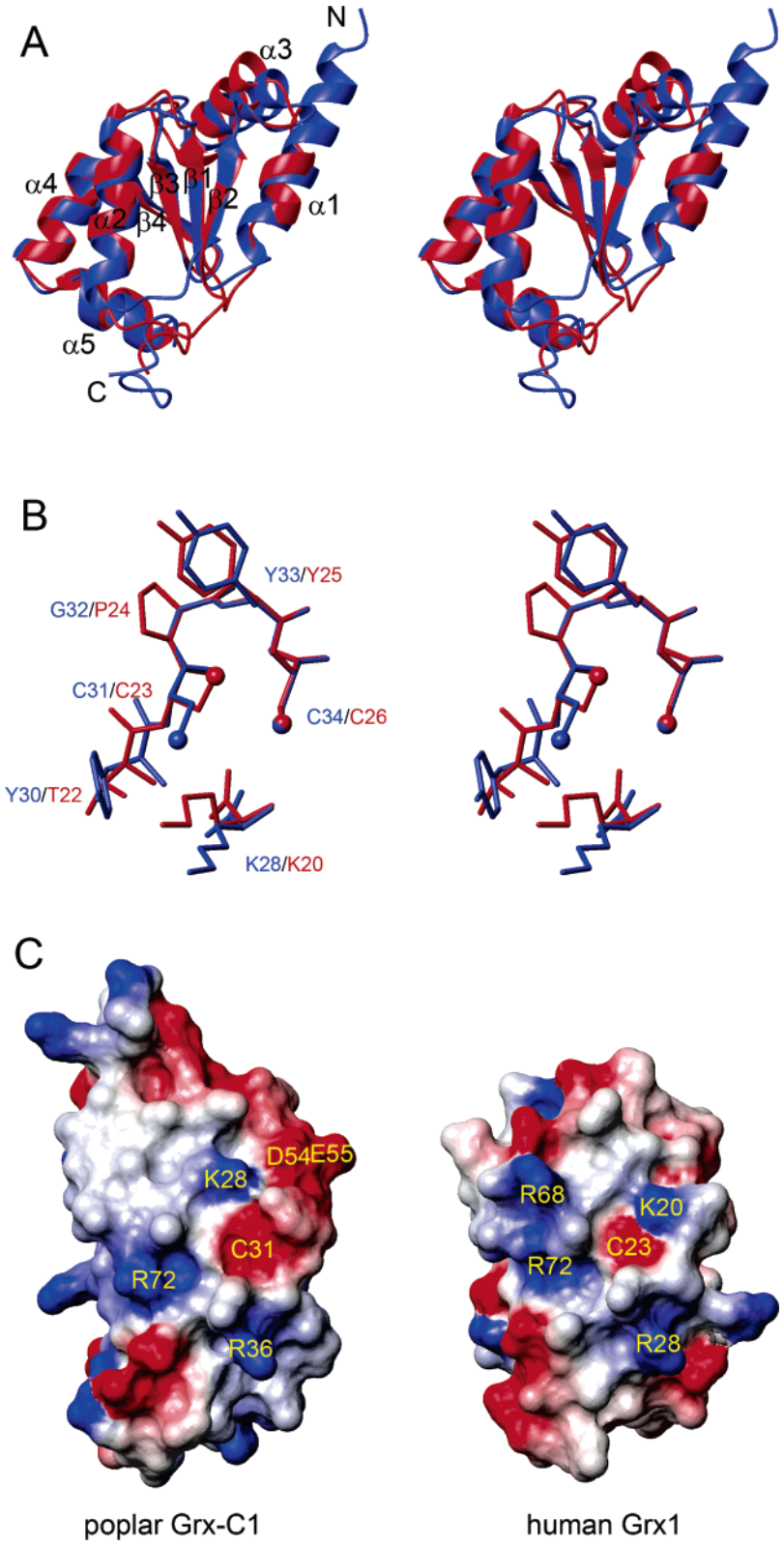


FIGURE 8: Structural comparison of poplar Grx-C1 and human Grx1. (A) Stereoview of the aligned structures of poplar Grx-C1 (blue) and human Grx1 (red). (B) Stereoview of the active site conformations of poplar Grx-C1 (blue) and human Grx1 (red). Only bonds between heavy atoms are shown for clarification. Structures are aligned using the backbone heavy atoms of active site residues. Sulfur atoms of cysteines are shown as spheres. (C) Electrostatic surfaces of poplar Grx-C1 (left) and human Grx1 (right). Charged residues near the active sites are indicated. The mean structure of human Grx1 was generated from PDB entry 1JHB using MOLMOL and was energy minimized with AMBER.

cysteines should be from one of the active site cysteines of each subunit. In the structure of apo Grx-C1, the side chain of the first active site cysteine is relatively exposed to the protein surface, and the second active site cysteine is almost completely buried. So, it is most possible that the first active site cysteines from two subunits serve as the other two ligands for the ISC in holo Grx-C1. Therefore, on the basis of our NMR studies, we proposed that the ISC in holo Grx-

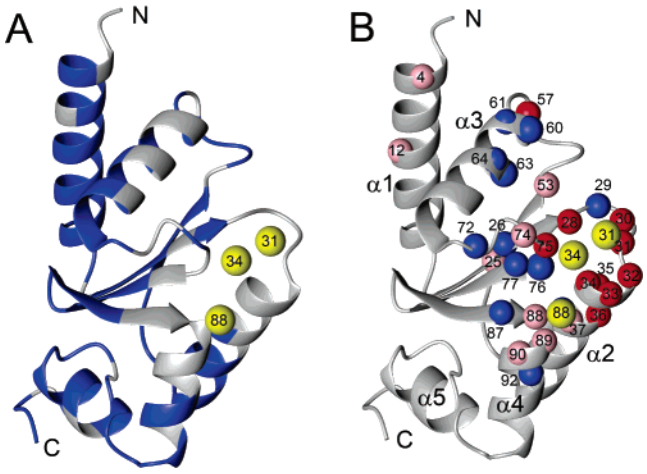


FIGURE 9: (A) Mapping of the residues with small $^{1}H$ and $^{15}N$ combined chemical shift differences (<0.1 ppm). These residues are indicated on a ribbon diagram of the poplar apo Grx-C1 structure in blue. The sulfur atoms of cysteines are shown as yellow spheres. (B) Mapping of residues with large chemical shift changes and/or the peak intensity changes in the 2D $^{1}H-^{15}N$ HSQC spectra of the structure. The nitrogen atoms corresponding to the missing peaks in holo Grx-C1 are shown as red spheres. The nitrogen atoms of residues with large intensity changes are shown as pink spheres. The nitrogen or carbon atoms of residues with large chemical shift changes, but no intensity change, are shown as blue spheres. The sulfur atoms of cysteines are shown as yellow spheres.

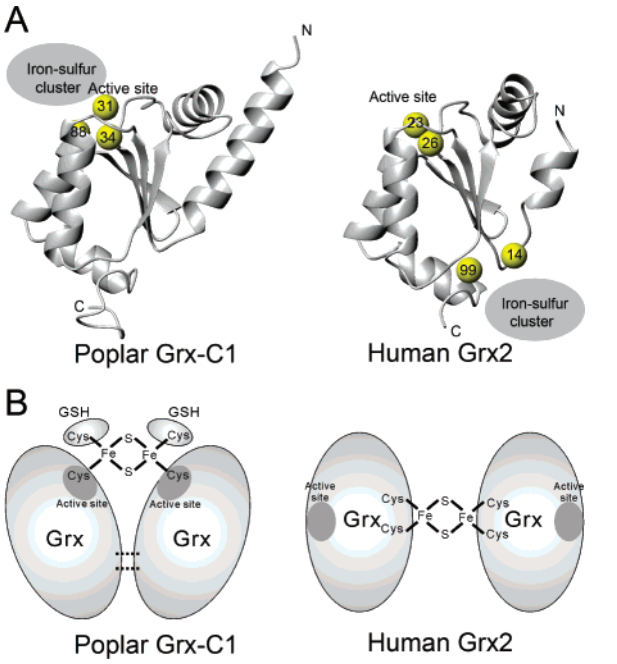


FIGURE 10: Comparison of the holo forms of poplar Grx-C1 and human Grx2. (A) Iron−sulfur cluster locations for holo poplar Grx-C1 and human Grx2. The structure of human Grx2 is obtained from homologous modeling. The sulfur atoms of cysteines are shown as yellow spheres labeled with residue numbers. (B) Illustrations of the coordination patterns of iron−sulfur clusters for holo poplar Grx-C1 and human Grx2.

C1 is coordinated by the cysteines from two GSHs and the first active site cysteines from two subunits.

The ISC coordination pattern in holo Grx-C1 is quite different from that of the holo form of human Grx2, although the ISCs in both Grxs are bridging two subunits. The two Grxs have two different ISC coordination patterns, and both of them are very unique. The ligands in human Grx2 were proposed to be the two non-active site cysteines that are located on opposite sides of the active site (Figure 10A). The ISC in holo Grx-C1 is coordinated by the active site cysteines along with the cysteines from two GSHs, and holo Grx-C1 has a novel structural and ISC coordination pattern (Figure 10B).

*Structure−Functional Implications.* Normally, one of the Fe(III) atoms in most [2Fe-2S]-type iron−sulfur proteins, such as ferredoxins, would be reduced to Fe(II) by the dithionite. It is unusual that the [2Fe-2S] cluster of holo Grx-C1 cannot be reduced by dithionite under anaerobic conditions and the cluster is lost when dithionite is added in the presence of oxygen. Similarly, human Grx2 also loses its [2Fe-2S] cluster upon dithionite reduction (*13*). The loss of ISC has been shown to play important roles in protein activity, such as in aconitase that catalyzes the stereospecific isomerization of citrate to isocitrate (*17*, *38*). The aconitase has a [4Fe-4S] cluster that serves as its enzymatic active site. However, the loss of the [4Fe-4S] cluster converts it into an iron regulatory protein (IRP), which is a translation regulator. Likewise, a regulatory role of the ISC for the enzyme activity and biological functions may be postulated for poplar Grx-C1.

Interestingly, it has recently been reported that an *E. coli* thioredoxin mutant, with a CACC active site sequence, can form a dimer with a bridging [2Fe-2S] cluster (*39*). The first two cysteines of the active site from both subunits serve as the ISC ligands. This thioredoxin mutant, fused to a leader peptide, can catalyze oxidation of protein disulfides in the periplasmic space and serve as a protein disulfide carrier to complement the activity of the DsbA/DsbB system in vivo. It is also found that both the [2Fe-2S] cluster and the third free cysteine are important for the function of this thioredoxin mutant, and the ISC is lost upon dithionite reduction.

If the holo poplar Grx-C1 indeed has two GSHs as ISC ligands, its situation would be quite similar to that of the CACC thioredoxin mutant, with one bridging [2Fe-2S] cluster and a free cysteine at the active site. Therefore, one could speculate that poplar Grx-C1 could possibly play a similar role in catalyzing the oxidation of protein disulfides in vivo.

The GSH molecules in holo poplar Grx-C1 should be very important for its function and regulation. GSH serves as glutaredoxin reductase and is the natural electron provider for the glutaredoxin. Holo Grx-C1 keeps the glutaredoxin and GSH together, and therefore, the GSH molecules can be utilized intermediately for the glutaredoxin function after the ISC falls off.

It would be more interesting to identify some unique features from the structure of poplar Grx-C1 to reveal the structure basis for its dual-form existence. As mentioned above, the structure of human Grx1 is quite similar to that of poplar Grx-C1. However, human Grx1 does not have an iron−sulfur protein form. When these two protein structures are compared, one notable difference is that the first active site cysteine thiolate for human Grx1 is surrounded by positive charges while that thiolate for poplar Grx-C1 is not completely surrounded by positive charges and one side of it is negatively charged (Figure 8C). Since the ISC is positively charged, one may suspect that formation of the ISC can benefit from the negative charge. In addition, the

active site sequence of poplar Grx-C1 is CGYC, which is different from the classical active site CPYC sequence in human Grx1. In general, glycine is more structurally flexible than proline. When the ISC is formed at the active site, the Grx active site may undergo local conformational changes and CGYC should be more favorable than CPYC in that sense. However, these structural differences are still minor and cannot reasonably explain why poplar Grx-C1 forms an iron−sulfur protein. Further biochemical studies are needed to reveal the detail and exact mechanism.

## ACKNOWLEDGMENT

All NMR experiments were carried out at the Beijing NMR Center. We thank Dr. Hongmei Wang, Dr. Hideaki Unno, and Dr. Yutaka Takahashi for their help in this work.

## REFERENCES

1. Fernandes, A. P., and Holmgren, A. (2004) Glutaredoxins: Glutathione-dependent redox enzymes with functions far beyond a simple thioredoxin backup system, *Antioxid. Redox Signaling 6*, 63−74.
2. Sodano, P., Xia, T. H., Bushweller, J. H., Bjornberg, O., Holmgren, A., Billeter, M., and Wuthrich, K. (1991) Sequence-specific $^{1}$H NMR assignments and determination of the three-dimensional structure of reduced *Escherichia coli* glutaredoxin, *J. Mol. Biol. 221*, 1311−1324.
3. Xia, T. H., Bushweller, J. H., Sodano, P., Billeter, M., Bjornberg, O., Holmgren, A., and Wuthrich, K. (1992) NMR structure of oxidized *Escherichia coli* glutaredoxin: Comparison with reduced *E. coli* glutaredoxin and functionally related proteins, *Protein Sci. 1*, 310−321.
4. Nordstrand, K., Sandstrom, A., Aslund, F., Holmgren, A., Otting, G., and Berndt, K. D. (2000) NMR structure of oxidized glutaredoxin 3 from *Escherichia coli*, *J. Mol. Biol. 303*, 423−432.
5. Xia, B., Vlamis-Gardikas, A., Holmgren, A., Wright, P. E., and Dyson, H. J. (2001) Solution structure of *Escherichia coli* glutaredoxin-2 shows similarity to mammalian glutathione-S-transferases, *J. Mol. Biol. 310*, 907−918.
6. Fladvad, M., Bellanda, M., Fernandes, A. P., Mammi, S., Vlamis-Gardikas, A., Holmgren, A., and Sunnerhagen, M. (2005) Molecular mapping of functionalities in the solution structure of reduced GRX4, a monothiol glutaredoxin from *Escherichia coli*, *J. Biol. Chem. 280*, 24553−24561.
7. Wang, Y., Amegbey, G., and Wishart, D. S. (2004) Solution structures of reduced and oxidized bacteriophage T4 glutaredoxin, *J. Biomol. NMR 29*, 85−90.
8. Katti, S. K., Robbins, A. H., Yang, Y., and Wells, W. W. (1995) Crystal structure of thioltransferase at 2.2 Å resolution, *Protein Sci. 4*, 1998−2005.
9. Sun, C., Berardi, M. J., and Bushweller, J. H. (1998) The NMR solution structure of human glutaredoxin in the fully reduced form, *J. Mol. Biol. 280*, 687−701.
10. Vlamis-Gardikas, A., and Holmgren, A. (2002) Thioredoxin and glutaredoxin isoforms, *Methods Enzymol. 347*, 286−296.
11. Lemaire, S. D. (2004) The glutaredoxin family in oxygenic photosynthetic organisms, *Photosynth. Res. 79*, 305−318.
12. Rouhier, N., Gelhaye, E., and Jacquot, J. P. (2004) Plant glutaredoxins: Still mysterious reducing systems, *Cell. Mol. Life Sci. 61*, 1266−1277.
13. Lillig, C. H., Berndt, C., Vergnolle, O., Lonn, M. E., Hudemann, C., Bill, E., and Holmgren, A. (2005) Characterization of human glutaredoxin 2 as iron−sulfur protein: A possible role as redox sensor, *Proc. Natl. Acad. Sci. U.S.A. 102*, 8168−8173.
14. Beinert, H. (2000) Iron−sulfur proteins: Ancient structures, still full of surprises, *J. Biol. Inorg. Chem. 5*, 2−15.
15. Sticht, H., and Rosch, P. (1998) The structure of iron−sulfur proteins, *Prog. Biophys. Mol. Biol. 70*, 95−136.
16. Beinert, H., Holm, R. H., and Munck, E. (1997) Iron−sulfur clusters: Nature's modular, multipurpose structures, *Science 277*, 653−659.
17. Kiley, P. J., and Beinert, H. (2003) The role of Fe−S proteins in sensing and regulation in bacteria, *Curr. Opin. Microbiol. 6*, 181−185.
18. Rodriguez-Manzaneque, M. T., Tamarit, J., Belli, G., Ros, J., and Herrero, E. (2002) Grx5 is a mitochondrial glutaredoxin required for the activity of iron/sulfur enzymes, *Mol. Biol. Cell 13*, 1109−1121.
19. Muhlenhoff, U., Gerber, J., Richhardt, N., and Lill, R. (2003) Components involved in assembly and dislocation of iron−sulfur clusters on the scaffold protein Isu1p, *EMBO J. 22*, 4815−4825.
20. Feng, Y., Rouhier, N., Jacquot, J. P., and Xia, B. (2005) Letter to the Editor: $^{1}$H, $^{15}$N, and $^{13}$C resonance assignments of reduced glutaredoxin C1 from *Populus tremula x tremuloides*, *J. Biomol. NMR 31*, 263−264.
21. Markley, J. L., Bax, A., Arata, Y., Hilbers, C. W., Kaptein, R., Sykes, B. D., Wright, P. E., and Wuthrich, K. (1998) Recommendations for the presentation of NMR structures of proteins and nucleic acids, *J. Biomol. NMR 12*, 1−23.
22. Delaglio, F., Grzesiek, S., Vuister, G. W., Zhu, G., Pfeifer, J., and Bax, A. (1995) NMRPipe: A multidimensional spectral processing system based on UNIX pipes, *J. Biomol. NMR 6*, 277−293.
23. Johnson, B. A., and Blevins, R. A. (1994) NMRView: A computer program for the visualization and analysis of NMR data, *J. Biomol. NMR 4*, 603−614.
24. Herrmann, T., Guntert, P., and Wuthrich, K. (2002) Protein NMR structure determination with automated NOE assignment using the new software CANDID and the torsion angle dynamics algorithm DYANA, *J. Mol. Biol. 319*, 209−227.
25. Duggan, B. M., Legge, G. B., Dyson, H. J., and Wright, P. E. (2001) SANE (Structure Assisted NOE Evaluation): An automated model-based approach for NOE assignment, *J. Biomol. NMR 19*, 321−329.
26. Cornilescu, G., Delaglio, F., and Bax, A. (1999) Protein backbone angle restraints from searching a database for chemical shift and sequence homology, *J. Biomol. NMR 13*, 289−302.
27. Pearlman, D. A., Case, D. A., Caldwell, D. A., Ross, W. R., Cheatham, T. E., III, DeBolt, S., Ferguson, D., Seibel, G., and Kollman, P. (1995) AMBER, a computer program for applying molecular mechanics, normal mode analysis, molecular dynamics and free energy calculations to elucidate the structures and energies of molecules, *Comput. Phys. Commun. 91*, 1−41.
28. Koradi, R., Billeter, M., and Wuthrich, K. (1996) MOLMOL: A program for display and analysis of macromolecular structures, *J. Mol. Graphics 14*, 51−55, 29−32.
29. Laskowski, R. A., Rullmannn, J. A., MacArthur, M. W., Kaptein, R., and Thornton, J. M. (1996) AQUA and PROCHECK-NMR: Programs for checking the quality of protein structures solved by NMR, *J. Biomol. NMR 8*, 477−486.
30. Schwede, T., Kopp, J., Guex, N., and Peitsch, M. C. (2003) SWISS-MODEL: An automated protein homology-modeling server, *Nucleic Acids Res. 31*, 3381−3385.
31. Gan, Z. R., and Wells, W. W. (1987) Identification and reactivity of the catalytic site of pig liver thioltransferase, *J. Biol. Chem. 262*, 6704−6707.
32. Mieyal, J. J., Starke, D. W., Gravina, S. A., and Hocevar, B. A. (1991) Thioltransferase in human red blood cells: Kinetics and equilibrium, *Biochemistry 30*, 8883−8891.
33. Nordstrand, K., Aslund, F., Meunier, S., Holmgren, A., Otting, G., and Berndt, K. D. (1999) Direct NMR observation of the Cys-14 thiol proton of reduced *Escherichia coli* glutaredoxin-3 supports the presence of an active site thiol-thiolate hydrogen bond, *FEBS Lett. 449*, 196−200.
34. Yang, Y. F., and Wells, W. W. (1990) High-level expression of pig liver thioltransferase (glutaredoxin) in *Escherichia coli*, *J. Biol. Chem. 265*, 589−593.
35. Lyon, R. P., and Atkins, W. M. (2001) Self-assembly and gelation of oxidized glutathione in organic solvents, *J. Am. Chem. Soc. 123*, 4408−4413.
36. Foloppe, N., and Nilsson, L. (2004) The glutaredoxin -C-P-Y-C- motif: Influence of peripheral residues, *Structure 12*, 289−300.
37. Prantner, A. M., Volkman, B. F., Wilkens, S. J., Xia, B., and Markley, J. L. (1997) Assignment of $^{1}$H, $^{13}$C, and $^{15}$N signals of reduced *Clostridium pasteurianum* rubredoxin: Oxidation state-dependent changes in chemical shifts and relaxation rates, *J. Biomol. NMR 10*, 411−412.

38. Beinert, H., Kennedy, M. C., and Stout, C. D. (1996) Aconitase as iron−sulfur protein, enzyme, and iron-regulatory protein, *Chem. Rev. 96*, 2335−2374.
39. Masip, L., Pan, J. L., Haldar, S., Penner-Hahn, J. E., DeLisa, M. P., Georgiou, G., Bardwell, J. C., and Collet, J. F. (2004) An engineered pathway for the formation of protein disulfide bonds, *Science 303*, 1185−1189.
40. Chenna, R., Sugawara, H., Koike, T., Lopez, R., Gibson, T. J., Higgins, D. G., and Thompson, J. D. (2003) Multiple sequence alignment with the Clustal series of programs, *Nucleic Acids Res. 31*, 3497−3500.
41. Gouet, P., Courcelle, E., Stuart, D. I., and Metoz, F. (1999) ESPript: Analysis of multiple sequence alignments in PostScript, *Bioinformatics 15*, 305−308.
42. Mulder, F. A., Schipper, D., Bott, R., and Boelens, R. (1999) Altered flexibility in the substrate-binding site of related native and engineered high-alkaline *Bacillus subtilisins*, *J. Mol. Biol. 292*, 111−123.

BI060444T